International Communications in Heat and Mass Transfer 125 (2021) 105327

Contents lists available at ScienceDirect

International Communications in Heat and Mass Transfer

journal homepage: www.elsevier.com/locate/ichmt

Experimental and normalized sensitivity based numerical analyses of a novel humidifier-assisted highly efficient indirect evaporative cooler

Muhammad Ahmad Jamil [a], Ben Bin Xu [a], Laurent Dala [a], Muhammad Sultan [b], Lin Jie [c], Muhammad Wakil Shahzad [a,d,*]

[a] Mechanical & Construction Engineering Department, Northumbria University, Newcastle Upon Tyne NE1 8ST, United Kingdom
[b] Department of Agricultural Engineering, Bahauddin Zakariya University, Bosan Road, Multan 60800, Pakistan
[c] Department of Engineering Science, University of Oxford, Oxford OX1 3PJ, United Kingdom
[d] Water Desalination and Reuse Centre, King Abdullah University of Science & Technology, Thuwal 23955-6900, Saudi Arabia

ARTICLE INFO

Keywords:
Indirect evaporative cooler (IEC)
Space cooling
Humidifier assisted IEC
Normalized sensitivity analysis

ABSTRACT

Indirect evaporative cooling technology has emerged as an energy-efficient, low-cost, and sustainable alternative to conventional air conditioning systems for space cooling. This is because of its significant (40–50%) energy-saving potential compared to ventilation, vapor compression cooling, and desiccant cooling systems. The current paper presents a novel humidifier-assisted regenerative indirect evaporative cooler that eliminates the use of hydrophilic surfaces within the system and mitigates the fouling propensity and water management issues. A generic cell of the proposed system is fabricated and tested for different operating scenarios along with the uncertainty propagation analysis. Thereafter, a normalized sensitivity analysis is performed to identify the most influential parameters on the cooler performance. The experimental data shows an effective cooling performance with a temperature drop of 20 °C of outdoor air and cooling capacity of 175 watts of 1800 mm × 300 mm generic cell. The cooling coefficient of performance was calculated as 44 and maximum effectiveness of 83.82% for the proposed configuration. The sensitivity analysis reveals scaling trends of the coefficient of performance in the following order of primary air inlet temperature > primary air outlet temperature > primary air velocity and the cooler effectiveness as secondary air outlet temperature > primary air inlet temperature > primary air humidity > primary air outlet.

1. Introduction

The efficient (i.e., low energy, environment friendly, and economical) air conditioning is becoming inevitable with the challenges from global warming, growing population, hikes in energy prices, and concerns about environmental degradations [1,2]. Air conditioning (AC) consumes 40% of commercial and 36% of residential buildings to maintain a comfortable working and living environment as shown in Fig. 1. By 2050, the AC energy is expected to be tripled as compared to 2019 and accordingly the AC units will ramp to 5.6 billion. This hike in the AC market means 10 AC units will be sold every second in the next 30 years [3–7].

These high energy requirements are equally contributed by the excessive use (in domestic, commercial, and industrial sectors) as well as endogenous inefficiency of conventional air conditioning systems [8,9]. The first chiller was invented by William Carrier in 1902 and since then it has only reached the coefficient of performance (COP) from 4–5 as shown by ASHRAE classifications in Fig. 2 [10].

The prime reason for the low energy efficiency is the simultaneous handling of sensible and latent loads which poses rigid thermal and pressure lifts across the compressor to maintain a finite heat transfer rate [11,12] coupled with the low performance of refrigerant compressors, only 14% efficiency level [13]. Because of these temperature limitations, no significant improvement in the energy efficiency of traditional cooling systems has been achieved for the past few decades [14,15]. Apart from being energy-intensive, these systems also involve chemical-

Abbreviations: AC, Air conditioning; COP, Coefficient of performance; EES, Engineering equation solver; EER, Energy efficiency ratio; HVAC, Heat ventilation and air conditioning; IEC, Indirect evaporative cooler; NSC, Normalized sensitivity coefficient; RC, Relative contribution; RH, Relative humidity, %; SC, Sensitivity coefficient.

* Corresponding author at: Mechanical & Construction Engineering Department, Northumbria University, Newcastle Upon Tyne NE1 8ST, United Kingdom.
E-mail address: muhammad.w.shahzad@northumbria.ac.uk (M.W. Shahzad).

https://doi.org/10.1016/j.icheatmasstransfer.2021.105327

Available online 18 May 2021

based refrigerants and are responsible for high carbon emissions [16]. Therefore, it is needful to develop an efficient, sustainable, and economical system to cope with rising cooling demands [17].

Non-conventional air-conditioning systems such as indirect evaporative cooling (IEC) technology have attained significant attention in recent times [18,19]. It utilizes the evaporative potential of air to produce cooling and water as a refrigerant [20]. It de-couples the latent and sensible cooling loads and offers flexibility to optimize each process individually [21]. The IEC differs from the conventional direct cooling devices e.g., cooling towers and swarm coolers in which air experiences changes in both the temperature and humidity ratio [22]. In IEC systems, the supply air flows through the dry channels which is being cooled by the air in parallel wet channels (with moist air) separated by a nonporous surface that allows only heat transfer [23,24]. Besides standalone systems, the IECs have also shown significant energy-saving potential upon integration with conventional cooling systems [25–29]. For instance, the integration of IECs with mechanical cooling systems can take 50–75% of the cooling load [30–32], increase COP by 9–12% [33] thus saving energy by 55–60% [34–36]. Therefore, various configurations of IEC based on flow arrangement, air injections, and water distributions have been proposed and tested by researchers [37,38]. A critical review of some recent studies on IEC is presented in Table 1.

The critical review suggests that the indirect evaporative coolers can significantly reduce the energy consumption of space cooling as a standalone system as well as a pre-cooler for conventional cooling systems. However, despite significant efforts, these are still at the development stage because of design and operational limitations. The major among them are high manufacturing cost, peeling-off of wicking material, fouling of porous hydrophilic surfaces (wick material) due to warm and humid environment, water management in the wet channel, leakages, and resistance to orthogonal heat transfer due to the number of resistances including nonconducting wick material. A conventional regenerative type of IEC including main components, flow directions, and associated limitations is presented in Fig. 3. The system proposed in this study satisfactorily addresses these issues by eliminating the wick material and rearranging the humidification system compared to conventional IECs. The proposed system is characterized by ease of manufacturing, operation, and maintenance, low energy and water consumption, and high heat transfer characteristics.

The current paper presents, a detailed experimental and an advanced normalized sensitivity-based analysis of the proposed system. This sensitivity analysis provides a closer insight into the response of performance parameters against input parameters. Therefore, it can identify the most influential parameters to improve system performance and future designs. It is also important to emphasize that the normalized sensitivity analysis composed in this study allows one-to-one comparison of parameters whose magnitude can vary significantly on a common platform which cannot be achieved in the conventional simple derivative based sensitivity coefficients. For this purpose, firstly, the experiments are conducted at assorted operating conditions to estimate effectiveness, cooling loads, and coefficient of performance. Secondly, the experimental data is analyzed numerically to investigate the uncertainty propagation in different measured variables. Lastly, a normalized sensitivity analysis is performed to estimate the influence of different input parameters on the performance of the proposed IEC. The sensitivity analysis model presented in the study can be used for a rigorous design of IECs as well as other related systems.

2. Materials and methods

2.1. System description

The proposed system consists of a novel Maisotsenko or M-cycle [62] based regenerative type indirect evaporative cooler generic cell as shown in Fig. 4. The process flow diagram presented in Fig. 5 of the system shows that the wet channel (secondary) air is humidified in a separate humidifier after purging from the dry (primary) channel at the outlet which is the main novelty compared to existing IEC systems. In the humidifier, water is sprayed through a fine mist nozzle which increases the RH of the air ~100% thus reducing its temperature to wet-bulb (T_{wb}). This cool and humid air is supplied to the wet channel. The dry and wet channels are separated by a thin (0.025 mm thick) Aluminum foil which promotes orthogonal heat transfer between the channels. A blower attached at the dry channel outlet creates induced draft flow in the dry channel and forced draft in the wet channel thus reducing the pressure losses and energy consumption. The psychrometric chart for the proposed system is presented in Fig. 6.

For continuous monitoring and data acquisition, a three-point sensor (FH400) measuring velocity, dry bulb temperature, and wet bulb temperature is used. The sensor is installed at the outdoor air duct, supply air duct, return air duct (refer to Sensor 1–4 in Fig. 4) and the relative humidity at all these points is calculated using the dry bulb and wet bulb data. Moreover, it is important to emphasize that, during experimentation, the humidity of outdoor air is controlled and maintained at (0.010 kg/kg) using a dehumidifier. Therefore, the experimentation allows the study of purge air ratio on the system performance independently.

Meanwhile, it is worth mentioning that the proposed IEC can satisfactorily address the major limitations in the conventional systems i.e., high manufacturing cost, peeling-off of wick material, fouling of porous hydrophilic surfaces, water management in the wet channel, leakages, and resistance to transverse heat transfer due to nonconducting wick material. These issues are resolved by replacing the wick material with a

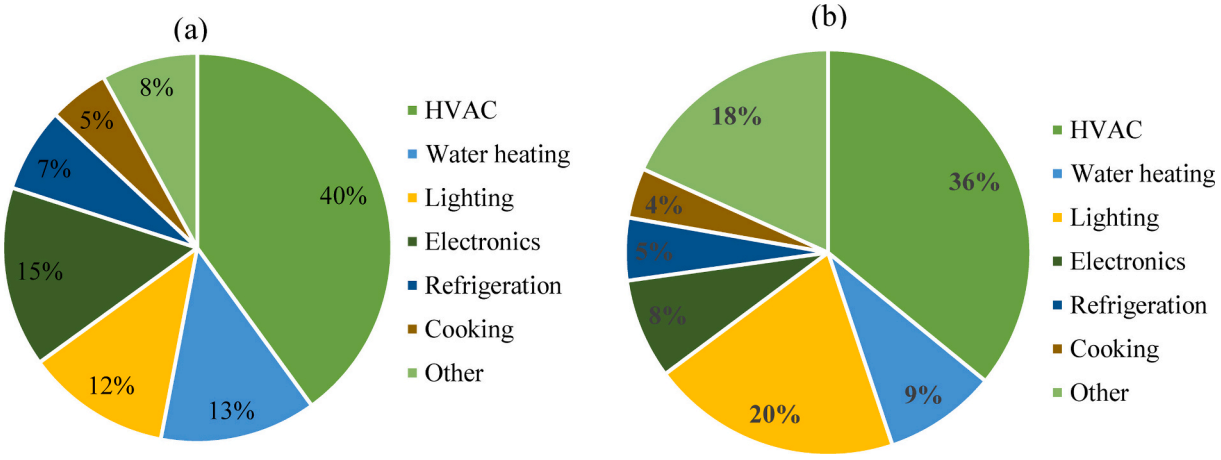

Fig. 1. Energy consumption distribution (a) commercial buildings, and (b) residential buildings [5–7].

high conductivity thin aluminum foil and placing the accessory components like a humidifier and water supply outside the cooler where these can be easily accessed without opening the channels. Therefore, the new cooler is characterized by ease of manufacturing, operation, and maintenance, low energy and water consumption, and high heat transfer characteristics. The design and operational data of the proposed IEC generic cell are presented in Table 2.

2.2. Performance indicators

The performance of indirect evaporative coolers is defined in terms of different parameters such as cooling capacity (Q), coefficient of performance (COP), wet bulb efficiency (η_{wb}), and cooler effectiveness (ε). The description of these parameters is given below.

The cooling capacity indicates the heat extracted from the primary/dry air in the dry channel and is calculated as,

$$\dot{Q}_{pa} = \dot{m}_{pa}\left(h_{pa,i} - h_{pa,o}\right) \tag{1}$$

The coefficient of performance (COP) is calculated on the cooling load and the power input i.e., the energy consumption of the blower.

$$COP = \frac{\dot{Q}_{pa}}{P_{electric}} \tag{2}$$

The wet-bulb effectiveness is calculated based on the primary air temperatures and secondary air wet-bulb temperature. As, ideally, the lowest temperature of outlet primary air is equal to the wet-bulb temperature of inlet secondary air so, the wet-bulb efficiency can give values greater than 100% which is not justified thermodynamically [44].

$$\eta_{wb} = \frac{T_{pa,i} - T_{pa,o}}{T_{pa,i} - T_{sa,wb,i}} \tag{3}$$

In this regard, a more appropriate measure of cooler effectiveness (without involving >100% misconceptions) is the cooler effectiveness defined based on the enthalpies. These enthalpies are calculated as a function of temperature, pressure, and humidity ratio.

$$\varepsilon = \frac{h_{pa,i} - h_{pa,o}}{h_{pa,o} - h_{sa,o}} \tag{4}$$

Some other parameters that are calculated for detailed analysis include flow area, Reynolds number, Nusselt number, heat transfer coefficient, and pressure drop in the channels. Because of the simple arrangement, the correlations developed for flow in parallel plates/rectangle can be employed as given below.

The effective number of plates are calculated by neglecting the outside plates which do not contribute to the heat transfer as

$$N_{eff} = N_{total} - 2 \tag{5}$$

The channel flow area is calculated using channel spacing and width of the plate,

$$A_{ch} = H \times W \tag{6}$$

The heat transfer area of a single plate is given below which can be multiplied by the effective number of plates for the total area.

$$A_{sp} = L \times W \tag{7}$$

The hydraulic diameter is given as,

$$D_h = \frac{4A_{ch}}{2\left(H + W\right)} \tag{8}$$

The Reynolds number is given as 1.

$$Re = \frac{V \times \rho \times D_h}{\mu} \tag{9}$$

Then the Nusselt number is calculated using the appropriate correlation of the form:

$$Nu = C_1 Re^{C_2} Pr^{C_3} \tag{10}$$

where, C_1, C_2, and C_3 depend upon the geometric and flow configurations. One such common relation used is the Dittus-Boelter empirical equation which is given as $Nu = 0.023\ Re^{0.8}\ Pr^{1/3}$ [63].

This Nu is used to calculate the heat transfer coefficient in each channel which is then used to calculate the overall heat transfer coefficient as given below.

$$\frac{1}{U} = \frac{1}{\lambda_{pa}} + \frac{1}{\lambda_{sa}} + \frac{\delta}{k_{plate}} \tag{11}$$

Similarly, the pressure drop is calculated on each side using the below-given equation:

$$\Delta P = 4f \times \frac{L \times N_{eff}}{D_{hyd}} \times \frac{G}{2\rho} \tag{12}$$

where G is the mass velocity in kg/m^{2}s [63].

2.3. Uncertainty propagation analysis

This analysis is conducted to estimate the error propagation in the response/calculated value of the output parameters (i.e., Q, η_{wb}, COP, ε etc.) due to the uncertainties in the measured values of the input parameters (e.g., T, V, ω etc.). The detailed specifications of the instruments used in the current system are presented in Table 3. It is also worth mentioning that the uncertainty in the response variable is calculated using the uncertainties in independent variables. For this purpose, all input parameters are modeled as a sum of their nominal value $\left(\overline{X}\right)$ and the uncertainty (U_X') about the nominal value as given below [64].

$$X = \overline{X} \pm U_X' \tag{13}$$

The corresponding uncertainty in the response variable Y due to U_X' is calculated as [65],

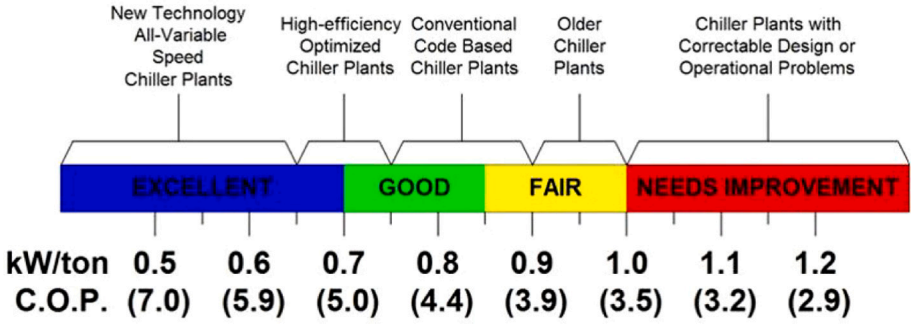

Fig. 2. Classifications of AC performance defined by ASHRAE [10].

Table 1
A comprehensive review of the latest IECs studies.

Study	Study type	Objective	Performance parameter	Remarks
Sun et al. [39]	Experimental	Effect of nozzle and spray strategy (porous ceramic IEC).	η_{wb} = 70–135%, ΔT_{pa} = 5–15 °C	The spiral nozzle has optimal water coverage. The best spray strategy is the 10–12 s spraying period and 1 min intermittent period.
Rajski [40]	Numerical	Effect of heat pipes integration with a gravity-assisted IEC.	η_{wb} = 70–105%, ΔT_{pa} = 6–15 °C, COP = 20–45	Inlet air conditions significantly affect the cooler performance and the suggested AFR is 0.3–0.5
Antonellis et al. [41]	Experimental	Effect of plate geometry on surface wettability.	η_{wb} = 40–50%, ΔP = 50–250 kPa	Plate geometry influences surface wettability and the best plate protrusion is reticulate.
Shahzad et al. [42]	Experimental	Effect of multipoint injection of working air.	COP = 37–78 (for only cooling)	The multipoint air injection improves performance by 3–4 °C
Zheng et al. [43]	Experimental and numerical	Effect of primary air condensation using FEM.	η_{wb} = 83% (no cond.), η_{wb} = 50% (cond.)	Higher primary air humidity increases water consumption, heat transfer but decreases η_{wb}.
Meng et al. [44]	Experimental	Effect of dry channel condensation.	η_{wb} = 48 to 80%	Thermal resistance due to condensation is non-negligible and it decreases η_{wb}.
Lv et al. [45]	Experimental	Effect of thermal resistance of condensate film thickness.	For $T_{pa,i}$ = 30–35 °C, δ_{film} = 0.085–0.17 μm	An increase in primary air temperature increases the condensate film thickness.
Chen et al. [46,47]	Numerical	Effect of primary air condensation.	$\eta_{wb} \leq$ 90%, Q = 140 kW/kg, $C_{enlargement}$ = 4.5	The most influential parameters on the η_{wb} are cooler Height > channel gap > AFR.
Guilizzoni et al. [48]	Experimental	Effect of water flow direction (top/side) and plate coatings.	η_{wb} = 78–84.4% (Top) and 57.3–69.6% (Side)	Wettability and η_{wb} of novel hydrophilic lacquer are higher than standard epoxy coating
Guo and Zheng, [49]	Experimental	Effect of sensible and latent heat transfer conditions.	η_{wb} = 50–66%, COP = 7–20 $\eta_{lat} \geq$ 45%, $\eta_{th} \geq$ 130%	The only COP can accurately measure IEC performance under all operating conditions.
Comino and Adana [50]	Numerical	Feasibility of IEC for net-zero energy building applications.	ΔT_{pa} = 16.28 °C, $Q_{cooling}$ = 8303 W, COP = 21	Regenerative IEC is recommended for low-cost space cooling
Antonellis et al. [51]	Experimental	Effect of water nozzles and airflow arrangements in IEC	η_{wb} = 82–84% (horizontal), η_{wb} = 48–66% (bottom)	Top and horizontal water flow arrangement gives the highest η_{wb} due to water distribution.
Antonellis et al. [52,53]	Experimental and numerical	IEC operating under data center operating conditions	η_{wb} = 50–85%., η_{db} = 62%, η_{sa}, = 20–62% (saturation)	ΔT_{pa} = 6 °C (hot and humid), ΔT_{pa} = 17 °C (cold and dry)
Wang et al. [54]	Experimental	Effect of porous ceramic tubes on IEC.	η_{wb} = ≤ 40%. COP = 20–34.9, Energy saving = 95%	η_{wb} improved with the increase of AFR with optimal value 0.9.
Duan et al. [55]	Experimental and numerical	Stud of a novel compact regenerative IEC.	η_{wb} = 96–107%, Q = 3.9–8.5 kW, EER = 10.6–19.7	The cooling capacity per unit volume is 62–108% higher than the conventional coolers.
Duan et al. [56]	Experimental	Effect of corrugated sheets.	η_{wb} = 55–106%, EER = 2.8 to 15.5	η_{wb} and EER of proposed cooler are 31% and 40% higher than the conventional.
Ahmad et al. [57]	Experimental	Effect of different controlled environmental conditions.	η_{wb} = 84–96%, η_{dp} = 58–67%, EER = 7.1–55.1	EER is directly proportional to the wet-bulb depression.
Lee and Lee [58]	Experimental	Effect of finned channels.	η_{wb} = 118–122%, η_{dp} = 75–90%	The maximum cooling capacity is achieved at a 30% purge air ratio.
Lin et al. [59]	Experimental and numerical	Effect of dehumidification of primary air on IEC.	η_{wb} = 125%, (low ω) η_{wb} = 86% (moderate ω)	Dehumidification of the supply air improved $Q_{cooling}$, and energy efficiency by 70% - 135%
Kabeel et al. [60]	Experimental	Effect of internal baffles, condenser, and a thin coating	Qcooling = 224.7 and 490.3 kW (for proposed IEC)	Proposed IEC with precooling, baffles, and coating has 35.4–54.2% higher cooling capacity
Chua et al. [61]	Numerical	Modified LMTD for IEC	η_{wb} = 82–90%	The best configuration is cross-flow of primary air with counter-flow of secondary air and water.
Current study	Experimental and numerical	Proposal and investigation of a novel humidifier assisted highly efficient regenerative IEC	Experimental: COP, η_{wb}, Normalized sensitivity coefficient and relative contribution coefficient for different input parameters	Focused to achieve a system with low manufacturing, operation, and maintenance costs, low energy, water consumption, and high heat transfer characteristics.

η_{wb}: wet bulb effectiveness, EER: energy efficiency ratio, Q: heat transfer rate, COP: coefficient of performance, ω: humidity ratio g/kg, δ: thickness.

$$U_Y' = \frac{dY}{dX} U_X' \tag{14}$$

For a multi-variate function $Y = Y(X_1, X_2, .., X_N)$, the U_Y' uncertainty in Y due to uncertainties in X is given by the root sum square product of the individual uncertainties computed to the first-order accuracy as [66],

$$U_Y' = \left\{ \left(\frac{\partial Y}{\partial X_1} U_{X_1}'\right)^2 + \left(\frac{\partial Y}{\partial X_2} U_{X_2}'\right)^2 + \cdots\cdots + \left(\frac{\partial Y}{\partial X_N} U_{X_N}'\right)^2 \right\}^{\frac{1}{2}} \tag{15}$$

2.4. Sensitivity analysis

The sensitivity analysis provides a closer insight into the response of performance parameters against input parameters [67]. It can be used to identify future work directions to improve system performance by targeting the most influential parameters. It is important to emphasize that the procedure for sensitivity analysis is nearly the same as that of uncertainty analysis with the only difference that the uncertainty term U' is replaced by the perturbation term U''. The value of perturbation is selected thus, Eqs. (2), (3), and (4) take the form [68].

$$X = \overline{X} \pm U_X'' \tag{16}$$

$$U_Y'' = \frac{dY}{dX} U_X'' \tag{17}$$

$$U_Y'' = \left\{ \left(\frac{\partial Y}{\partial X_1} U_{X_1}''\right)^2 + \left(\frac{\partial Y}{\partial X_2} U_{X_2}''\right)^2 + \cdots\cdots + \left(\frac{\partial Y}{\partial X_N} U_{X_N}''\right)^2 \right\}^{\frac{1}{2}} \tag{18}$$

It is important to mention that each partial derivative term in Eq. (18), represents the sensitivity coefficient (SC). It indicates the sensitivity of response parameters to a small change in the respective independent parameter [69]. However, a more appropriate and reliable method of presenting the sensitivity analysis results is through dimensionless Normalized Sensitivity Coefficients (NSC) [70]. It allows a one-to-one comparison of parameters whose magnitude can vary significantly [71]. These dimensionless NSC terms are calculated by normalizing the uncertainties in Y and X by their nominal values. After normalization, the general form of sensitivity equation in terms of NSC and normalized uncertainty (NU) is given as [72].

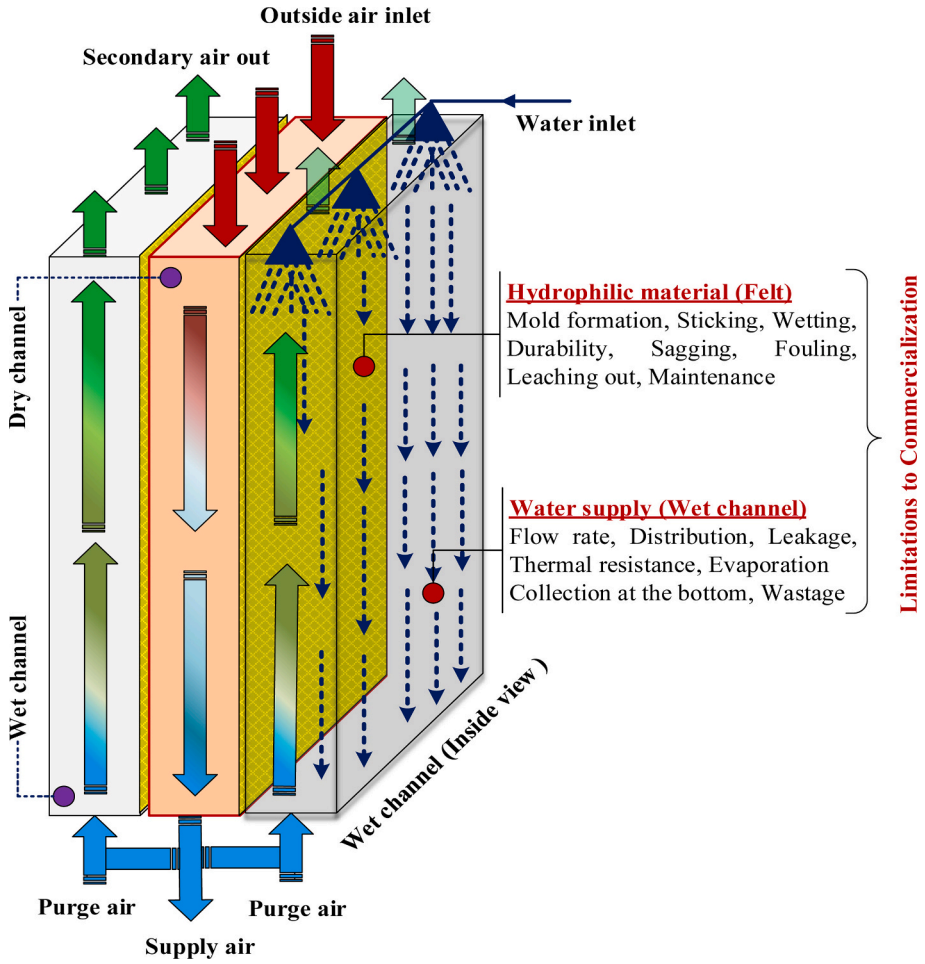

Fig. 3. Conventional regenerative IEC parts, working, and limitations.

$$\frac{U''_Y}{\overline{Y}} = \left[\sum_{i=1}^{N} \left(\frac{\partial Y}{\partial X_i} \frac{\overline{X}_i}{\overline{Y}} \right)^2 \left(\frac{\overline{U''_{X_i}}}{\overline{X}_i} \right)^2 \right]^{1/2} \quad (19)$$

For each response parameter, the above general equation can be modified in terms of independent parameters. Such as, for wet bulb effectiveness η_{wb}, the above equation can be given as:

$$\frac{U''_\varepsilon}{\overline{\varepsilon}} = \left[\left(\frac{\partial \varepsilon}{\partial T_{pi}} \frac{\overline{T}_{pi}}{\overline{\varepsilon}} \right)^2 \left(\frac{U''_{T_{pi}}}{\overline{T}_{pi}} \right)^2 + \left(\frac{\partial \varepsilon}{\partial T_{po}} \frac{\overline{T}_{po}}{\overline{\varepsilon}} \right)^2 \left(\frac{U''_{T_{po}}}{\overline{T}_{po}} \right)^2 + \left(\frac{\partial \varepsilon}{\partial T_{si}} \frac{\overline{T}_{si}}{\overline{\varepsilon}} \right)^2 \left(\frac{U''_{T_{si}}}{\overline{T}_{si}} \right)^2 + \left(\frac{\partial \varepsilon}{\partial T_{so}} \frac{\overline{T}_{so}}{\overline{\varepsilon}} \right)^2 \left(\frac{U''_{T_{so}}}{\overline{T}_{so}} \right)^2 \right]^{1/2} \quad (20)$$

Besides NSC, the other important parameter that predicts the dominant perturbation/ uncertainty contributors is the Relative Contribution (RC) [71]. It combines the sensitivity coefficients with the actual perturbation/uncertainty and is given as the square of the product of SC and perturbation/uncertainty, normalized by the square of the uncertainty in the response variable [72].

$$RC = \frac{\left(\frac{\partial Y}{\partial X_i} U''_{X_i} \right)^2}{U''^2_Y} \quad (21)$$

3. Solution strategy and assumptions

The above-mentioned set of equations for thermodynamic, uncertainty and sensitivity analyses are solved using an EES-based numerical code. In the first step, the input data from the experimental setup consisting of velocity, temperatures, and geometric parameters are provided. Then the thermophysical properties at terminal points of the dry and wet channels are calculated as a function of temperature, pressure, and humidity ratio using EES library routine-AirH$_2$O. The values of COP and effectiveness calculated from the code are validated with the experimental results. Thereafter, the code is employed to study the effect of different input parameters on the performance parameters. The analysis is based on the following assumptions: (a) steady-state operation, (b) insignificant longitudinal heat conduction, (c) uniform heat transfer coefficients, and (d) no thermal energy source or sink in the cooler section. The solution flow chart is presented in Fig. 7.

4. Results and discussion

4.1. Experimentation

The proposed generic cell is fabricated and tested over a range of operating conditions in terms of purge air ratio and outdoor air temperature. The effect of operational parameters is studied on the performance of IEC generic cell in terms of supply air temperatures, cooling capacity, coefficient of performance, and cooler effectiveness. Fig. 8 shows that an increase in purge air ratio decreased the supply air

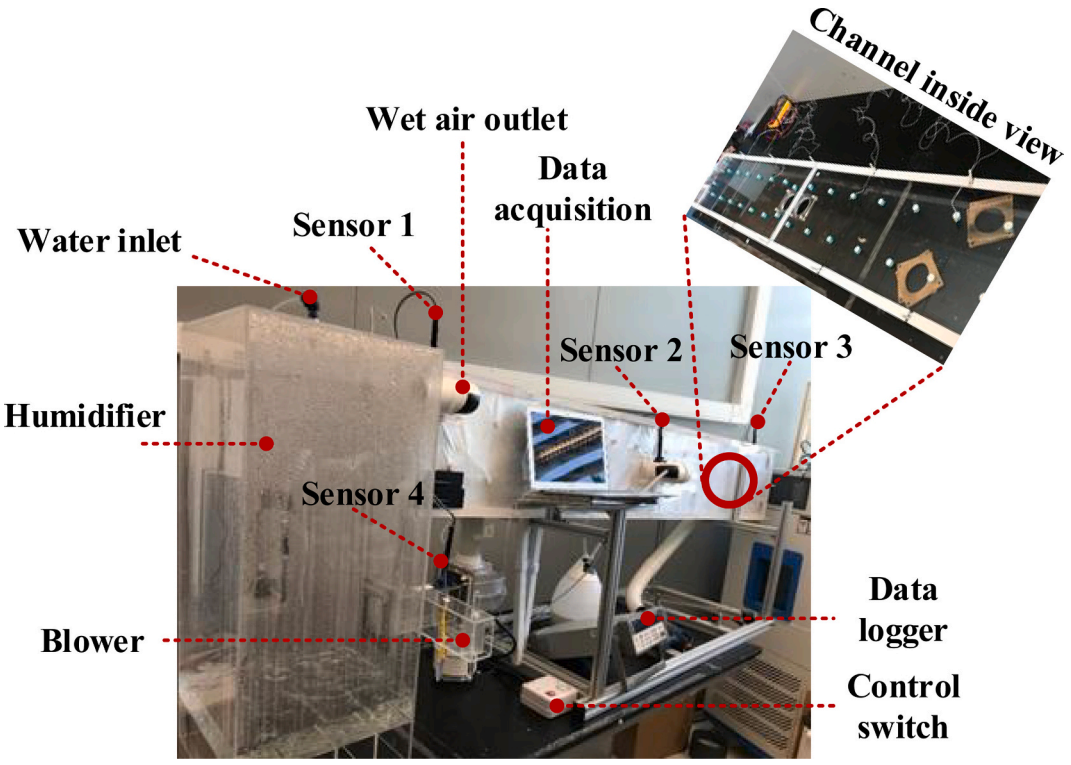

Fig. 4. Generic cell experimental setup.

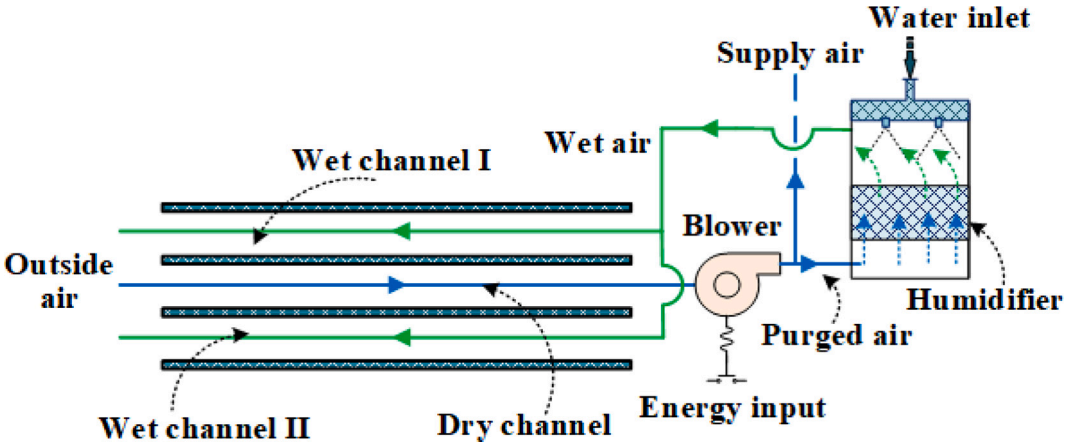

Fig. 5. Process flow diagram of proposed IEC.

temperature because of the high heat transfer rate at higher flow rates in the wet channel. Moreover, it is important to mention that the IEC is a passive machine, and its performance is directly controlled by the outdoor air humidity and purge air ratio. Since in the current analysis, the outdoor air humidity is maintained at 0.010 kg/kg using a dehumidifier, therefore the performance is governed by purge air ratio only. So, the analysis showed that the cooler performs better at higher purge air ratios producing low supply air temperatures.

Fig. 9 presents the effect of outdoor air temperature and purge air ratio on the cooling capacity of the generic cell. It is observed that the maximum cooling capacity of ~175 watts is achieved at the highest outdoor air temperature (i.e., 43 °C) and purge air ratio (i.e., 55%). At the same purge air, the cooling capacity decreased to 140-watt, 129-watt, 99-watt, and 41-watt as the outdoor air temperature reduced to 38 °C, 33 °C, and 27 °C, respectively. Meanwhile, the cooling capacity also decreased with decreasing the purge air ratio due to the low heat extraction rate from the dry channel. It is important to emphasize that any cooling capacity can be achieved by stacking the required number of generic cells based on the capacity of a single cell at the specified operating conditions. However, the optimal purge air ratio and outside air temperature should be selected for minimum investment.

The variation in the coefficient of performance against purge air ratio and outdoor air temperature is presented in Fig. 10. It is worth mentioning that the COP presented here is only for cooling and does not involve any dehumidification process. Therefore, the COP values appeared to be high i.e., up to 43–44. It is observed that the highest performance of the cooler is achieved at the maximum outdoor air temperature and the purge air ratio. It is also seen that the COP decreased significantly ~20–30% with a decrease in the outdoor air temperature by 5–6 °C at the same purge air. A similar trend with slightly different percentage reduction can be observed for other purge air ratios. This significant decrease in the COP values is due to the

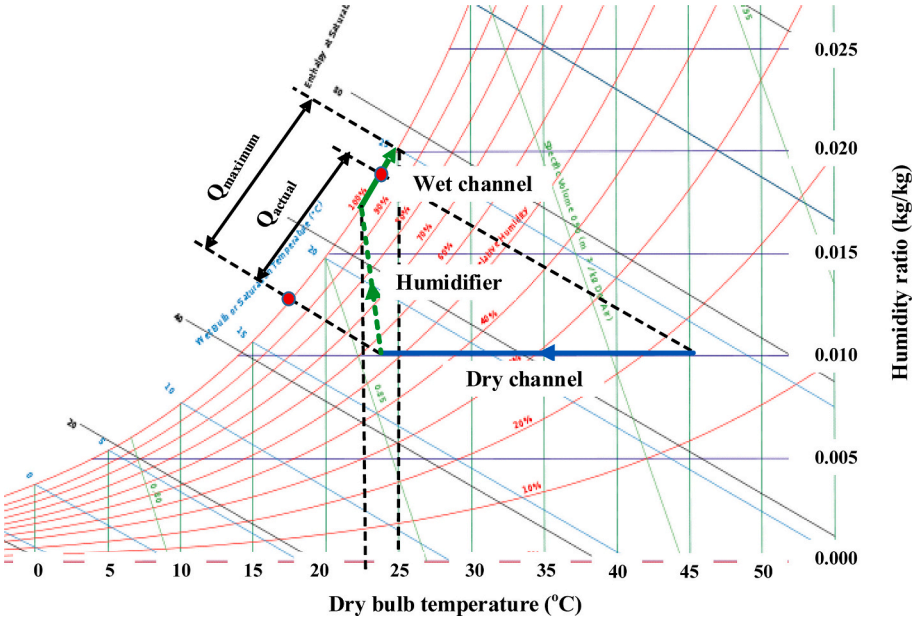

Fig. 6. Psychrometric description of proposed IEC.

Table 2
Design and operational parameters of the proposed generic cell.

Parameter	Value
Generic cell effective length, *L*, mm	1800
Generic cell effective width, *W*, mm	280
Separator Aluminium foil thickness, *δ*, mm	0.025
Dry and wet channels height (spacing), *H*, mm	5
Purge air ratio, *r*, %	35, 45, 55
Outdoor air temperature, °C	27, 33, 38, 43
Outdoor air humidity, ω, kg/kg	0.010
Outdoor air velocity, m/s	5.18
Wet air velocity in the wet channel, m/s	1.7, 2.25, 2.8

Table 3
Details of sensors and specifications installed in the IEC test cell.

Parameter	Sensor specification	Accuracy
Humidity	Humidity temperature dew point meter Company: Fisher Scientific Measuring range: 10 to 100%	± 0.5%
Temperature	Thermistors Company: OMEGA Measuring range: 0 to 80 °C & 0 to 100 °C	± 0.15 °C
Air velocity	Thermal flow probe air velocity meter Company: Testo (model:425) Measuring range: 0 to 20 m/s	± 0.03 m/s

decrease in the desired output i.e., heat transfer rate from the primary air as the blower power (desired input) is taken constantly i.e., 4-W. Meanwhile, it is also important to note that integration of the low COP dehumidification process (depending upon sensible heat ratio normally 1 for thermally driven and 3 for MVC system) with the cooler will significantly reduce the overall COP to 10–15. However, this COP is still significantly higher than the conventional air conditioning systems (COP 4–5). A similar trend can be observed for cooler effectiveness against purge air ratio and the outdoor air temperature as illustrated in Fig. 11. The maximum cooler effectiveness is calculated to be 83.82% at the highest outdoor air temperature and purge ratio.

Even though supply air temperature varied from 22-25 °C with various purge air ratios, still the system can maintain a comfortable environment as presented by Victor Olgyay and Givoni showed in Fig. 12 [73–76].

4.2. Uncertainty propagation analysis

The uncertainty propagation studied over an appropriate range of input parameters is presented in Fig. 13. It is observed that the total uncertainty propagation in the calculated parameters i.e., COP is ±0.5151, ε is ±1.702, η_{wb} is ±0.8959 and Q is ±0.00206 which is <2% different than measured parameters. Moreover, no significant variation is observed over the range of each parameter. As shown in Fig. 4 (a-c), the uncertainty in ε varied marginally from ±0.5181 to ±0.582 for COP from ±0.3104 to ±0.3054 and η_{wb} from ±0.08522 to ±0.05194 when $T_{pa,i}$ varied from 40 to 45 °C. Meanwhile, the uncertainty in COP due to inaccuracy of velocity meter is ±0.2553 and does not vary with changing V_{pa} values.

4.3. Sensitivity analysis

4.3.1. Preliminary indications

The findings of sensitivity analysis are presented in the form of sensitivity coefficient (SC), Normalized Sensitivity Coefficients (NSC), Relative Contribution (RC), and finally sorting the parameters in descending importance (Γ↓). In this regard, Table 4 presents the sensitivity of COP on different input parameters i.e., primary air inlet/outlet temperatures ($T_{pa,i}/T_{pa,o}$), secondary air inlet/outlet temperatures ($T_{sa,i}/T_{sa,o}$), primary/secondary air velocity (V_{pa}/V_{sa}), and humidity ratio of primary air (ω_{pa}). It is observed that the COP is the most sensitive to $T_{pa,i}$ with NSC = 4.285 followed by $T_{pa,o}$, and V_{pa} with NSCs of 1.396, and 0.999, respectively. The other parameters are almost insensitive to COP, however, their NSCs follow the order as $\omega_{pa} > T_{sa,i} > V_{sa} > T_{sa,o}$. While the RC follows the order as $T_{pa,o} > T_{pa,i} > V_{pa}$, and other parameters have a negligible contribution.

Similarly, the sensitivity of cooler effectiveness (ε) to different operational parameters is presented in Table 5. The most influential parameter in this regard is observed to be the $T_{sa,o}$ with NSC of 14.1 followed by $T_{pa,i}$, ω_{pa}, $T_{pa,o}$ with NSCs of 4.59, 0.766, and 0.098, respectively. While the other parameters are almost insignificant in the calculation of ε. In case of wet bulb effectiveness (η_{wb}) the sensitivity of the parameters follow the order as $T_{pa,o} > T_{sa,i} > T_{pa,i}$, with respective NSCs of 1.306, 0.949, and 0.0286 (refer Table 6). While the cooling load (Q_{pa}) is the most affected by $T_{pa,i}$ followed by $T_{pa,o}$, and V_{pa}, as

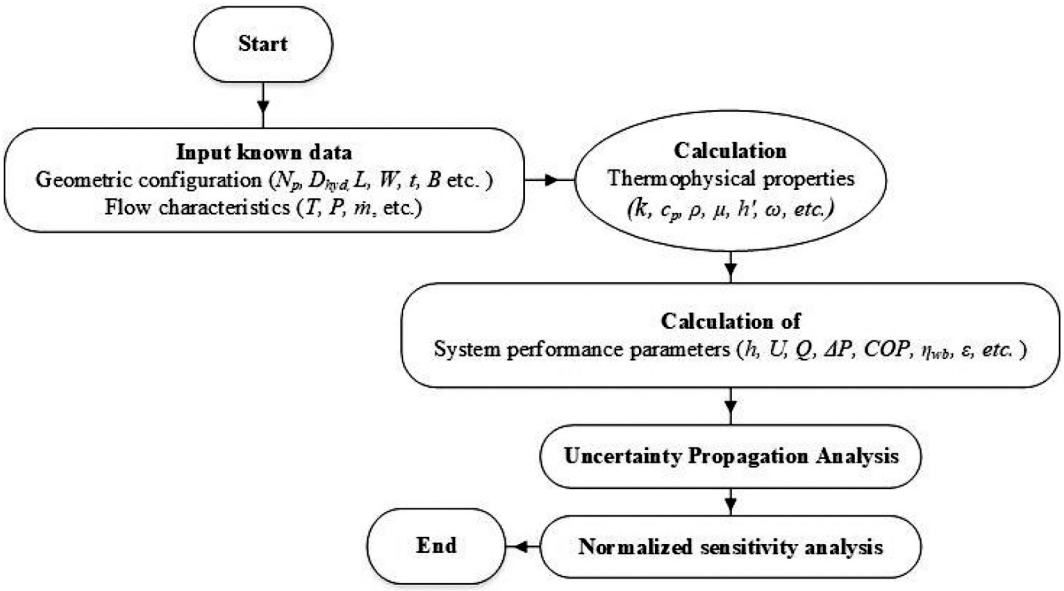

Fig. 7. Solution flow chart.

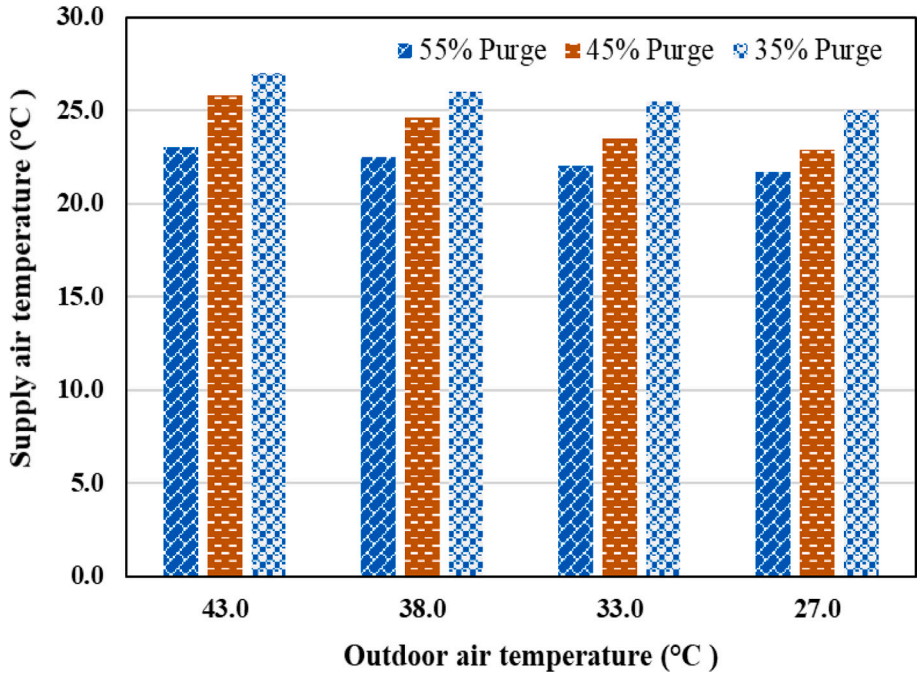

Fig. 8. Effect of outdoor air temperature on the supply air temperature.

demonstrated in Table 7.

4.3.2. NSC parametric study

After a detailed preliminary identification of the most influential input parameters in terms of NSC and RC, the variation in NSCs over a range of respective parameters are studied. Fig. 14 shows the variation in NSC of the COP and ε against inlet temperature of primary air keeping other parameters constant. It is observed that the values COP and ε is increased by increasing the inlet temperature of primary air because of the difference between the inlet and outlet temperature increases. However, the combined effect of all other constant parameters and perturbation causes the NSC of COP and ε to decrease by increasing the inlet temperature of primary air as shown in Fig. 15. Therefore, it indicates that the sensitivity of COP and ε over $T_{pa,i}$ decreases at higher values.

Fig. 16 shows the variation of NSC of the COP and η_{wb} against the outlet temperature of primary air keeping the other operating parameters constant. It is seen that the values of COP and η_{wb} decreased due to a decrease in the difference between the inlet and outlet temperature of primary air. However, the overall impact of constant quantities and perturbation causes to increase in the NSC of COP and η_{wb}. It means that the COP and η_{wb} will be more sensitive to the $T_{pa,o}$ at its higher values. Similarly, Fig. 17 illustrates the variation of NSC of effectiveness (ε) against the humidity ratio of primary air (ω_{pa}). It is observed that the

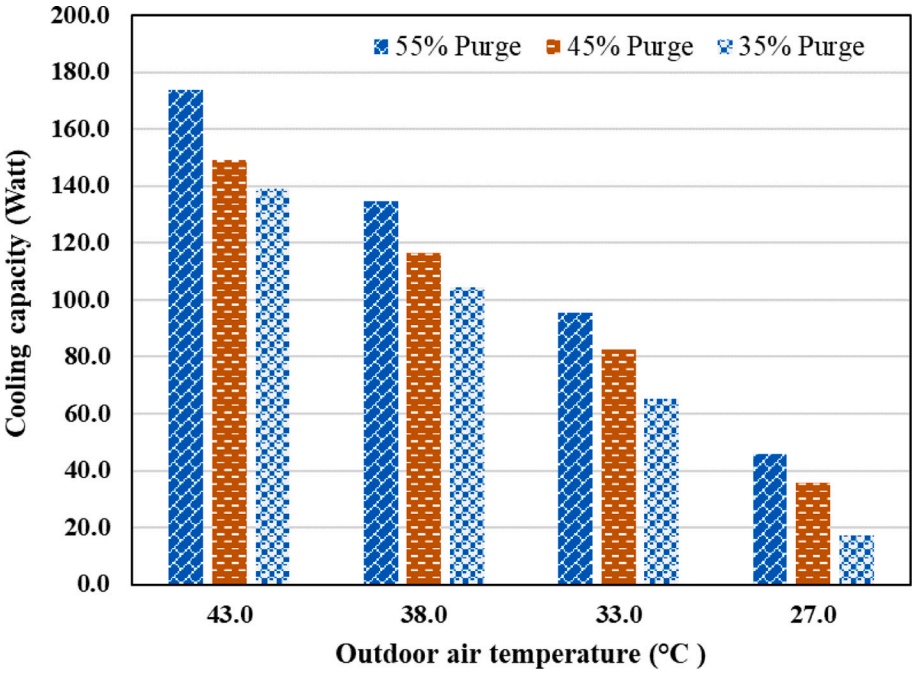

Fig. 9. Effect of outdoor air temperature on the cooling capacity.

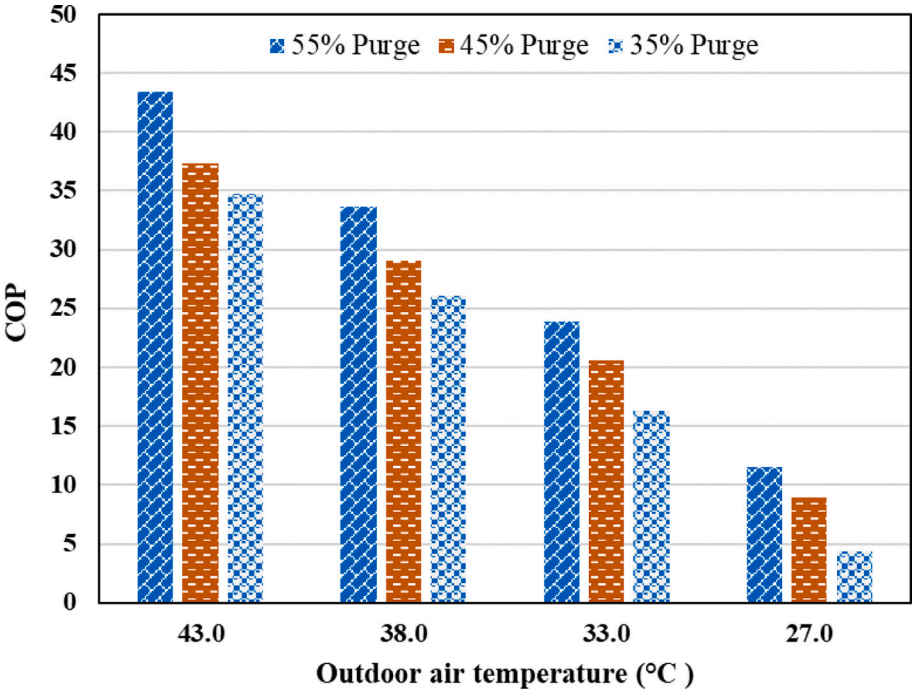

Fig. 10. Effect of outdoor air temperature on the coefficient of performance.

values ε increased by increasing ω_{pa} because the difference between inlet and outlet enthalpies of primary air is increased. The overall impact of other quantities and constant perturbation lead to an increase in the NSC of ε with increasing ω_{pa}. It suggests that at higher values of ω_{pa}, ε will be more sensitive to the primary air humidity. Some similar trends can be observed for NSCs of effectiveness, wet bulb efficiency, and cooling load against primary and secondary air inlet and outlet temperatures as illustrated in Figs. 18-20.

5. IEC development status and future roadmap

The status of indirect evaporative cooling technology highlighting major types, applications, performance indicators, limitations, and future roadmap is summarized in Fig. 21. The assessment of existing systems suggests that despite significant studies, several limitations hinder the commercial-scale development of IEC systems. Major among these included operational reliability, large area requirements, and high manufacturing and maintenance cost. The proposed system reasonably

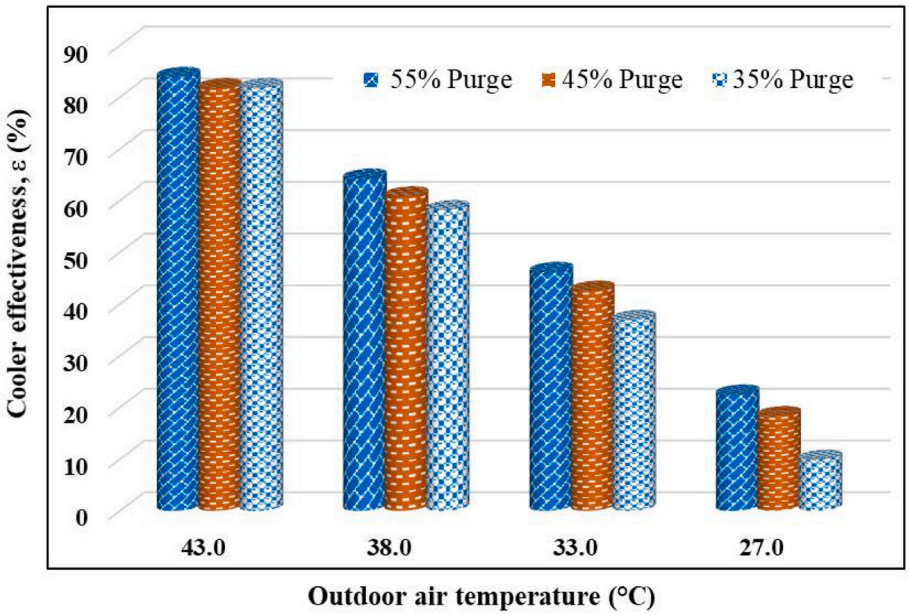

Fig. 11. Effect of outdoor air temperature on the cooler effectiveness.

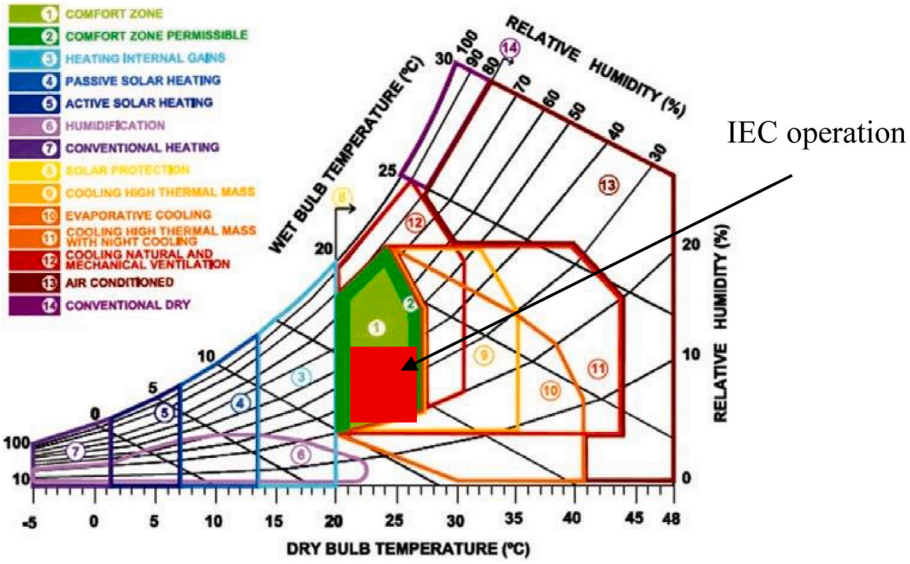

Fig. 12. Comfortable zones on psychrometric chart presented by Givoni in 1969 [73–76].

addressed these by eliminating the wicking material that reduced the maintenance issues as well as increased the heat transfer rate. Moreover, the water showering process is carried out in a separate humidifier which reduced the water consumption, leakage issues, and liquid film thermal resistance in the heat transfer process. Moreover, the effectiveness of the proposed cooler is comparable to the existing systems (85–90%).

6. Conclusion

A novel regenerative type of indirect evaporative cooler is proposed, fabricated, and tested at assorted operating conditions. The main objective of the system is to overcome the major limitations in the conventional IECs that include high water wastage, reliability of wicking material, the thermal resistance of water film, fouling, and high maintenance cost. The performance of the cooler is measured in terms of supply air temperature, cooling capacity, coefficient of performance, and effectiveness. Thereafter, a normalized sensitivity analysis is conducted to investigate the influence of important input parameters on these performance parameters. The major findings of the study under-considered operating conditions are as follows.

- The proposed IEC can satisfactorily address the major limitations in the conventional IECs by replacing the wick material with a high conductivity thin aluminum foil and placing the accessory components like a humidifier and water supply outside the cooler where these can be easily accessed without opening the channels.
- The lowest supply air temperature is achieved at the highest outdoor air temperature and purge air ratio because of the evaporative potential of air which is maximum at higher temperatures.
- The maximum cooling capacity of the cooler is recorded as ~175 watts at the highest outside air temperature of 43 °C and purge air ratio of 55%. The cooling capacity decreased to 140-watt, 129-watt, 99-watt, and 41-watt as the outside air temperature reduced to 38 °C,

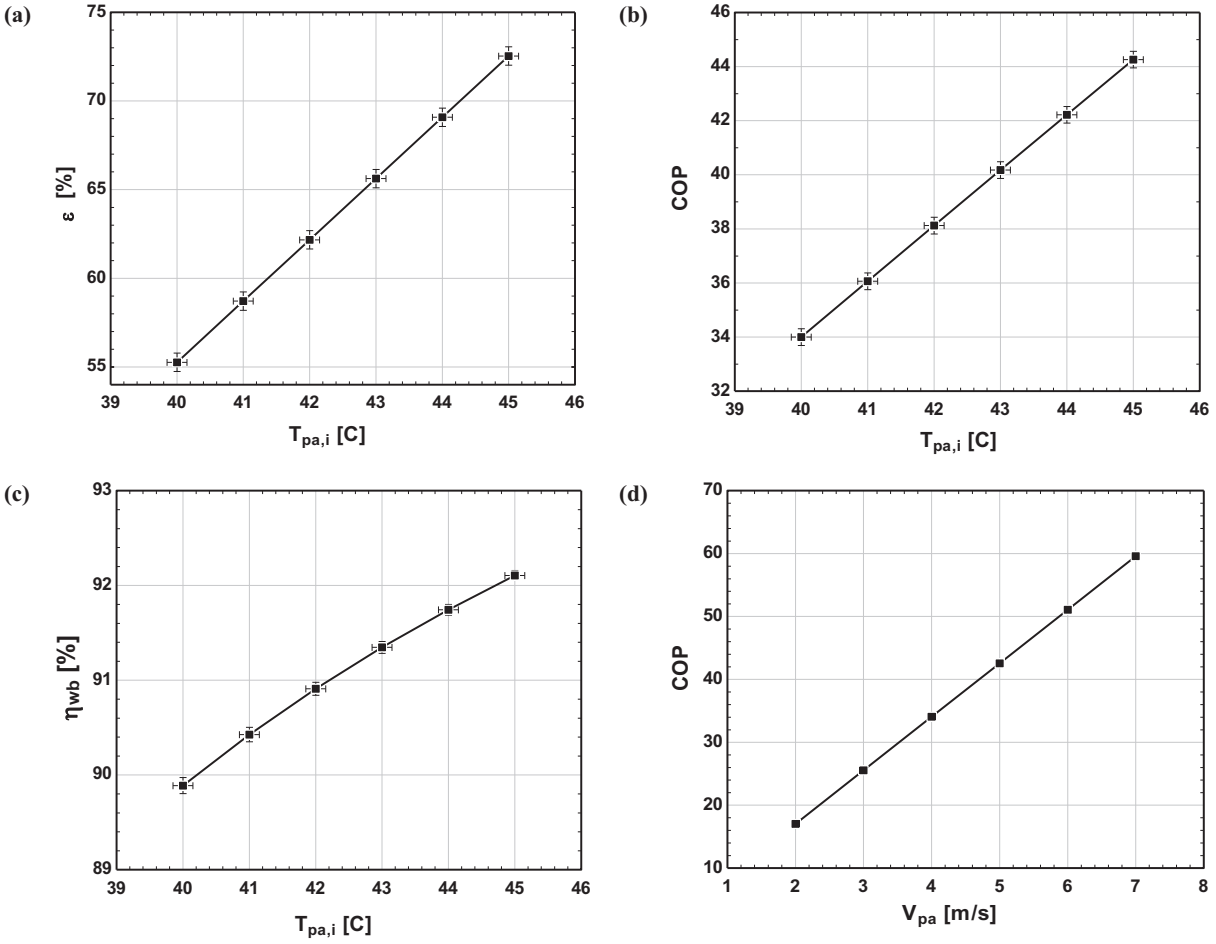

Fig. 13. Uncertainty propagation in (a) ε versus $T_{pa,i}$, (b) COP versus $T_{pa,i}$, (c) η_{wb} versus $T_{pa,i}$, and (d) COP versus V_{pa}.

Table 4
The sensitivity of the coefficient of performance (COP) to different parameters.

Variable	U_X''	$\overline{X}$	SC	NSC	RC (%)	Γ↓
$T_{pa,i}$	1 °C	45	4.145	4.285	45.60	$T_{pa,i}$
$T_{pa,o}$	1 °C	24	4.748	1.396	52.23	$T_{pa,o}$
$T_{sa,i}$	1 °C	22.2	3×10^{-32}	7×10^{-33}	3.4×10^{-31}	V_{pa}
$T_{sa,o}$	1 °C	25.7	0	0	0	ω_{pa}
V_{pa}	1%	5.2	0.195	0.999	2.154	$T_{sa,i}$
V_{sa}	1%	2.86	1.2×10^{-35}	6×10^{-35}	1.3×10^{-34}	V_{sa}
ω_{pa}	1%	0.01	1.12×10^{-06}	5×10^{-6}	1.2×10^{-5}	$T_{sa,o}$

Table 5
The sensitivity of effectiveness (ε) to different parameters.

Variable	U_X''	$\overline{X}$	SC	NSC	RC (%)	Γ↓
$T_{pa,i}$	1 °C	45	11.93	4.592	9.498	$T_{sa,o}$
$T_{pa,o}$	1 °C	24	0.900	0.098	0.716	$T_{pa,i}$
$T_{sa,i}$	1 °C	22.2	0	0	0	ω_{pa}
$T_{sa,o}$	1 °C	25.7	112.36	14.10	89.46	$T_{pa,o}$
V_{pa}	1%	5.2	4.8×10^{-35}	1.2×10^{-71}	3.8×10^{-35}	V_{pa}
V_{sa}	1%	2.86	0	0	1.3×10^{-34}	$T_{sa,i}$
ω_{pa}	1%	0.01	0.403	0.766	0.321	V_{sa}

Table 6
The sensitivity of wet bulb efficiency (η_{wb}) to different parameters.

Variable	U_X''	$\overline{X}$	SC	NSC	RC (%)	Γ↓
$T_{pa,i}$	1 °C	45	0.119	0.0286	0.336	$T_{pa,o}$
$T_{pa,o}$	1 °C	24	19.23	1.306	53.89	$T_{sa,i}$
$T_{sa,i}$	1 °C	22.2	16.34	0.949	45.77	$T_{pa,i}$
$T_{sa,o}$	1 °C	25.7	0	0	0	$T_{sa,o}$
V_{pa}	1%	5.2	0	0	0	ω_{pa}
V_{sa}	1%	2.86	0	0	0	V_{pa}
ω_{pa}	1%	0.01	0	0	0	V_{sa}

Table 7
The sensitivity of cooling load (Q_{pa}) to different parameters.

Variable	U_X''	$\overline{X}$	SC	NSC	RC (%)	Γ↓
$T_{pa,i}$	1 °C	45	6.6×10^{-5}	4.287	45.60	$T_{pa,i}$
$T_{pa,o}$	1 °C	24	7.6×10^{-5}	1.397	52.24	$T_{pa,o}$
$T_{sa,i}$	1 °C	22.2	0	0	0	V_{pa}
$T_{sa,o}$	1 °C	25.7	0	0	0	ω_{pa}
V_{pa}	1%	5.2	3.1×10^{-6}	1.001	2.155	$T_{sa,i}$
V_{sa}	1%	2.86	0	0	0	$T_{sa,o}$
ω_{pa}	1%	0.01	1.8×10^{-11}	5.7×10^{-6}	1.2×10^{-5}	V_{sa}

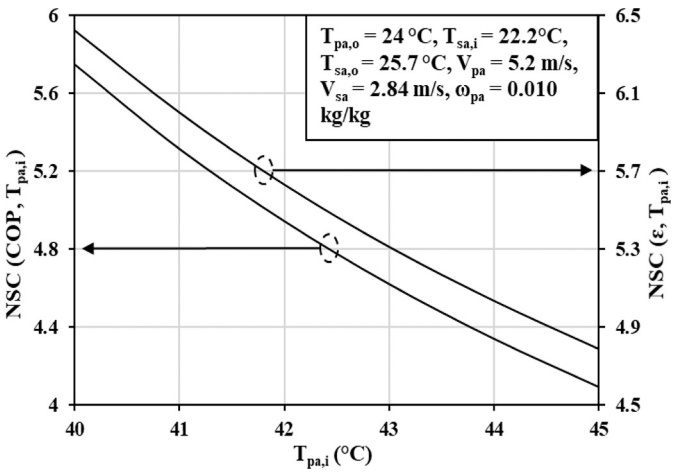

Fig. 14. Variation in NSC of the COP and ε against $T_{pa,i}$.

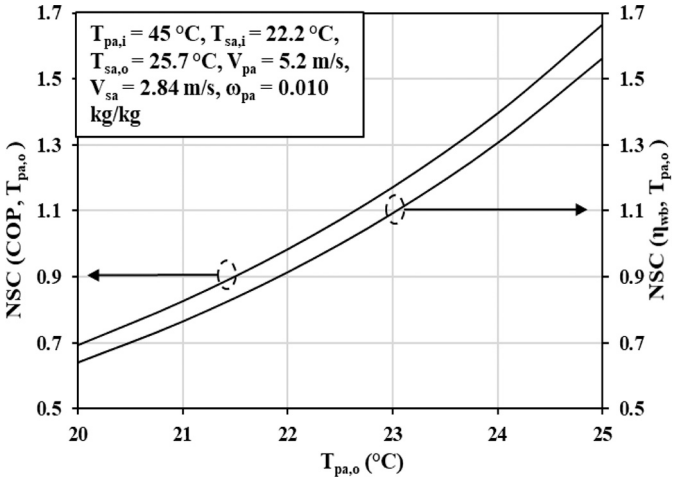

Fig. 15. Variation in NSC of the COP and η_{wb} against $T_{pa,o}$.

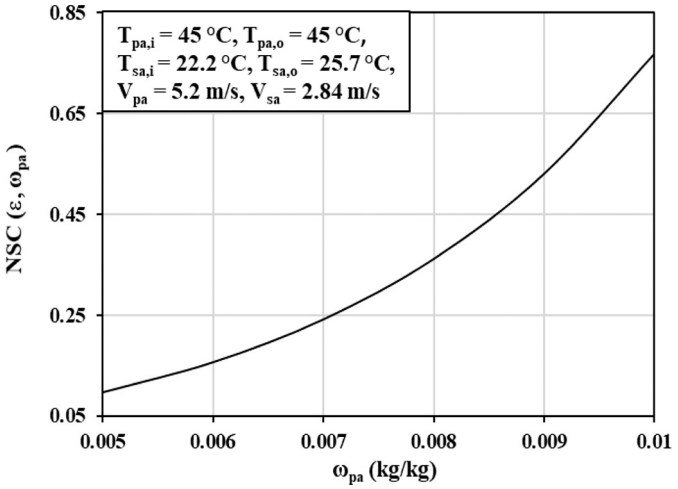

Fig. 16. Variation in NSC of ε against ω_{pa}.

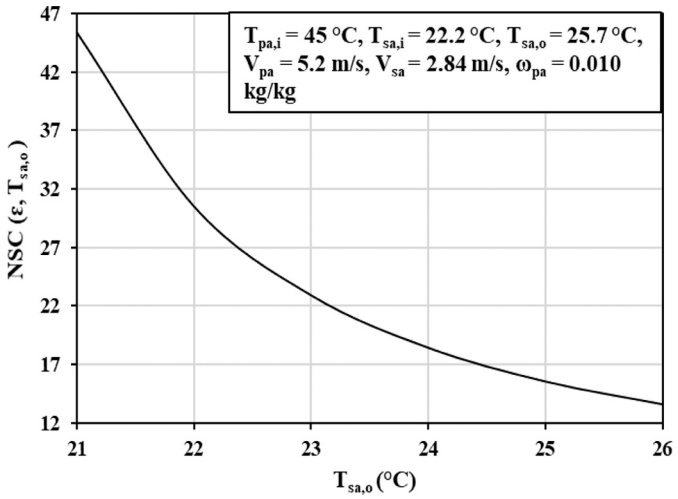

Fig. 17. Variation of NSC of in ε against $T_{sa,o}$.

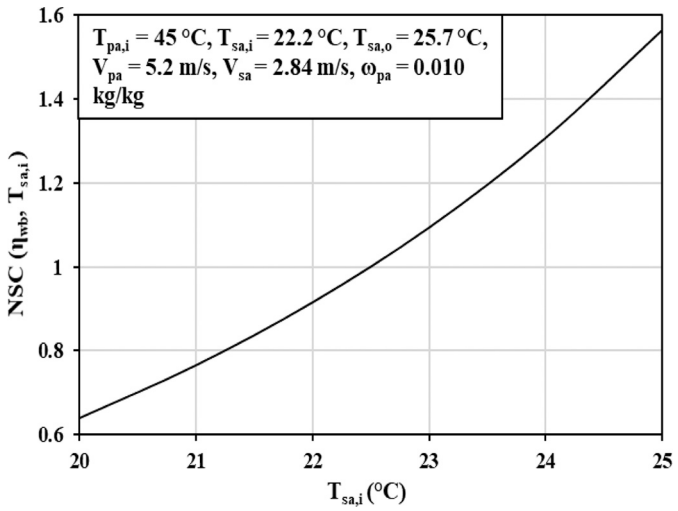

Fig. 18. Variation of NSC of η_{wb} against $T_{sa,i}$.

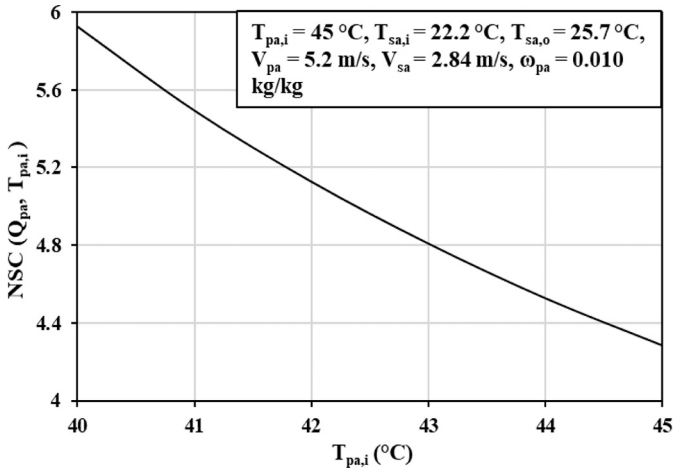

Fig. 19. Variation in NSC of cooling load against $T_{pa,i}$.

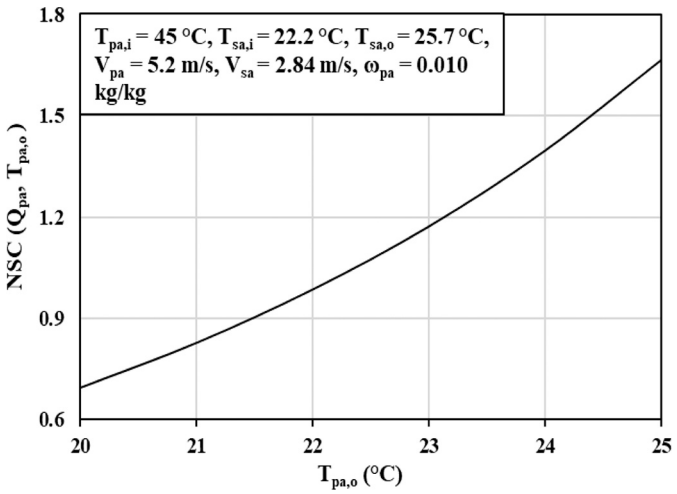

Fig. 20. Variation in NSC of cooling load to $T_{pa,o}$.

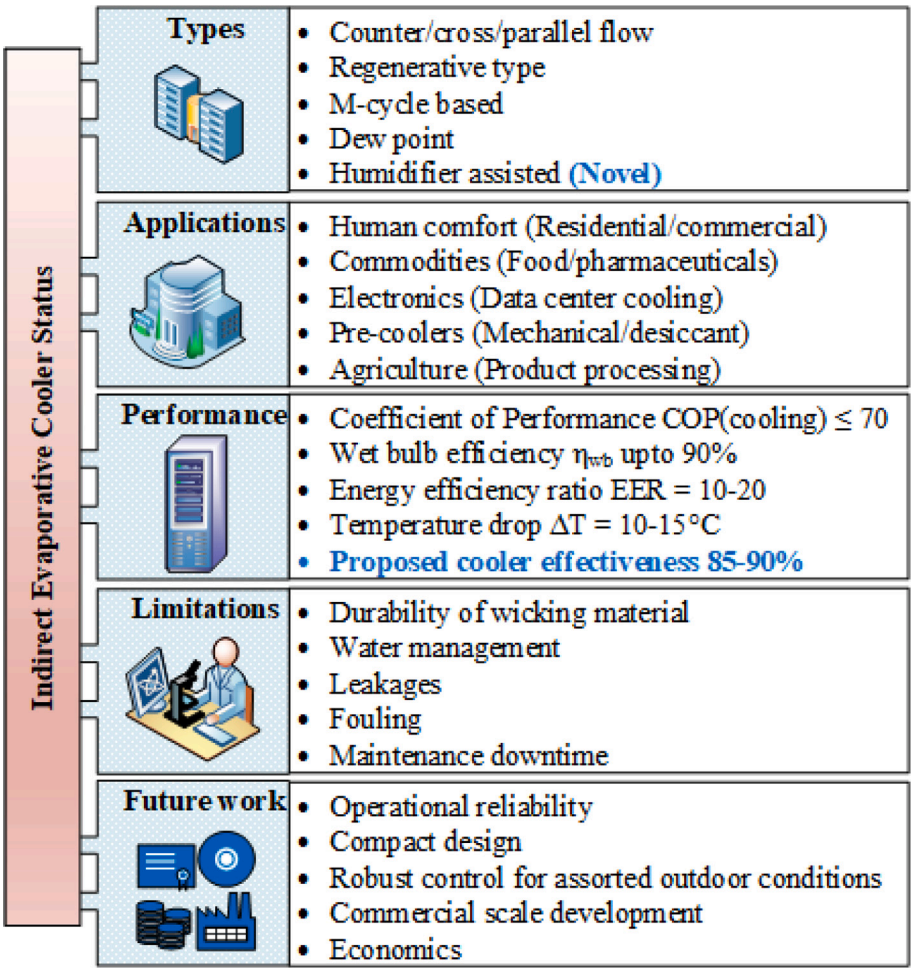

Fig. 21. IEC development status and future roadmap.

33 °C, and 27 °C, respectively at the same purge air ratios. Meanwhile, the cooling capacity also decreased with decreasing purge air ratio due to the low heat extraction rate from the dry channel.

- The maximum COP (for cooling only) is calculated as high as ~43–44 which decreased significantly (~20–30%) with decreasing outdoor air temperature by 5–6 °C at the same purge air ratio. The overall COP (cooing +dehumidification) is expected to hover around 10–15. The maximum cooler effectiveness is 83.82% which is also at the highest outdoor air temperature.
- The sensitivity analysis reveals that the coefficient of performance is sensitive to the operating parameters in the following order $T_{pa,i} > T_{pa,o} > V_{pa}$ and the cooler effectiveness as $T_{sa,o} > T_{pa,i} > \omega_{pa}, > T_{pa,o}$.
- The parametric analysis showed that the sensitivity of COP and ε decreased against increasing primary air inlet temperature, that of COP and η_{wb} increased against increasing the primary air outlet temperature and that of ε increased against primary air humidity ratio. These variations in sensitivity coefficients are because of the overall impact of other quantities and constant perturbations.

Nomenclature

A_{ch}	channel flow area, mm^2
A_{sp}	single plate heat transfer area, mm^2
D_h	hydraulic diameter, mm
f	friction factor
G	mass velocity, kg/m^2s
H	channel height, mm
h	enthalpy, j/kg
k	thermal conductivity, W/mK
L	length, mm
N	number of plates
P	pressure, pa
Pr	Prandtl number
Q	cooling capacity/heat transfer, W
Re	Reynolds number
r	purge ratio, %
T	temperature, °C
V	velocity, m/s
W	width, mm

Subscripts

i	inlet
lat	latent
o	outlet
pa	primary air
sa	secondary air
th	thermal
wb	wet bulb

Greek letter

Δ	change in quantity
Γ↓	descending importance
δ	film thickness, μm
ω	humidity ratio, kg/kg
μ	viscosity, kg/ms
ε	effectiveness
ρ	density, kg/m^3
λ	heat transfer coefficient, W/m^2K

Declaration of Competing Interest

None.

Acknowledgment

The authors would like to thank KCI project by OSR KAUST Saudi Arabia and support provided by Northumbria University, UK under reference # RDF20/EE/MCE/SHAHZAD and MCE QR Steering Fund 2020/21.

References

[1] M. Ali, W. Ahmad, N.A. Sheikh, H. Ali, R. Kousar, T. ur Rashid, Performance enhancement of a cross flow dew point indirect evaporative cooler with circular finned channel geometry, J. Build. Eng. (2020), 101980, https://doi.org/10.1016/j.jobe.2020.101980.
[2] C. Zhan, Z. Duan, X. Zhao, S. Smith, H. Jin, S. Riffat, Comparative study of the performance of the M-cycle counter-flow and cross-flow heat exchangers for indirect evaporative cooling - paving the path toward sustainable cooling of buildings, Energy 36 (2011) 6790–6805, https://doi.org/10.1016/j.energy.2011.10.019.
[3] IEA Reports, The Future of Cooling: Opportunities in Energy-efficient Air Conditioning. https://www.iea.org/publications/freepublications/publication/The_Future_of_Cooling.pdf, 2017.
[4] B. Fikri, E. Sofia, N. Putra, Experimental analysis of a multistage direct-indirect evaporative cooler using a straight heat pipe, Appl. Therm. Eng. 171 (2020) 115133, https://doi.org/10.1016/j.applthermaleng.2020.115133.
[5] K.J. Chua, M.R. Islam, N. Kim Choon, M.W. Shahzad, Advances in Air Conditioning Technologies, Springer Singapore, Singapore, 2021, https://doi.org/10.1007/978-981-15-8477-0.
[6] Real Prospects for Energy Efficiency in the United States, The National Academies Press, 2010. https://www.nap.edu/catalog/12621/real-prospects-for-energy-efficiency-in-the-united-states. (Accessed 23 January 2021).
[7] Air Conditioning Use Emerges as One of the Key Drivers of Global Electricity-demand Growth, News - IEA, 2018. https://www.iea.org/news/air-conditioning-use-emerges-as-one-of-the-key-drivers-of-global-electricity-demand-growth. (Accessed 23 January 2021).
[8] G. Todesco, Chillers + Lighting + TES: Why CFC Chiller Replacement Can Be Energy-savings Windfall 47, ASHRAE, 2005, pp. 18–27.
[9] F.J.R. Martínez, E.V. Gómez, R.H. Martín, J.M. Gutiérrez, F.V. Diez, Comparative study of two different evaporative systems: an indirect evaporative cooler and a semi-indirect ceramic evaporative cooler, Energy Build. 36 (2004) 696–708.
[10] F. Oliveira, A. Ukil, Comparative performance analysis of induction and synchronous reluctance motors in chiller systems for energy efficient buildings, IEEE Trans. Ind. Inform. 15 (2019) 4384–4393, https://doi.org/10.1109/tii.2018.2890270.
[11] R.Z. Wang, X. Yu, T.S. Ge, T.X. Li, The present and future of residential refrigeration, power generation and energy storage, Appl. Therm. Eng. 53 (2013) 256–270, https://doi.org/10.1016/j.applthermaleng.2012.02.034.
[12] S.J. Oh, K.C. Ng, K. Thu, W. Chun, K.J.E. Chua, Forecasting long-term electricity demand for cooling of Singapore's buildings incorporating an innovative air-conditioning technology, Energy Build. 127 (2016) 183–193, https://doi.org/10.1016/j.enbuild.2016.05.073.
[13] J. Glol, D. Oppelt, C. Becker, J. Heubes, Green Cooling Technologies, Market Trends in Selected Refrigeration and Air Conditioning Subsectors, Deutsche Gesellschaft für Internationale Zusammenarbeit (GIZ) GmbH, 2015.
[14] Z. Duan, C. Zhan, X. Zhang, M. Mustafa, X. Zhao, Indirect evaporative cooling: past, present and future potentials, Renew. Sust. Energ. Rev. 16 (2012) 6823–6850, https://doi.org/10.1016/j.rser.2012.07.007.
[15] A. Stefano, D.A. Cesare, M. Joppolo, L. Samanta, M. Luca, Experimental analysis of a cross flow indirect evaporative cooling system, Energy Build. 121 (2016) 130–138, https://doi.org/10.1016/j.enbuild.2016.03.076.
[16] B.I. Campbell, A. Kalanki, S. Sachar, B. Hartley, Solving the Global Cooling Challenge: How to Counter the Climate Threat from Room Air Conditioners. https://rmi.org/wp-content/uploads/2018/11/Global_Cooling_Challenge_Report_2018.pdf, 2018.
[17] V. Eveloy, D.S. Ayou, Challenges, and Future Opportunities, With Emphasis on Cooling-dominated Regions, Energies 12 (2019) 235, https://doi.org/10.3390/en12020235.
[18] Q. Liu, C. Guo, X. Ma, Y. You, Y. Li, Experimental study on total heat transfer efficiency evaluation of an indirect evaporative cooler, Appl. Therm. Eng. 174 (2020) 115287, https://doi.org/10.1016/j.applthermaleng.2020.115287.
[19] Z. Duan, C. Zhan, X. Zhang, M. Mustafa, X. Zhao, B. Alimohammadisagvand, A. Hasan, Indirect evaporative cooling: past, present and future potentials, Renew. Sust. Energ. Rev. 16 (2012) 6823–6850, https://doi.org/10.1016/j.rser.2012.07.007.
[20] O. Khalid, M. Ali, N.A. Sheikh, H.M. Ali, M. Shehryar, Experimental analysis of an improved Maisotsenko cycle design under low velocity conditions, Appl. Therm. Eng. 95 (2016) 288–295, https://doi.org/10.1016/j.applthermaleng.2015.11.030.
[21] J. Lin, D.T. Bui, R. Wang, K.J. Chua, On the exergy analysis of the counter-flow dew point evaporative cooler, Energy 165 (2018) 958–971, https://doi.org/10.1016/j.energy.2018.10.042.
[22] S.J. Oh, M.W. Shahzad, M. Burhan, W. Chun, C. Kian Jon, M. KumJa, K.C. Ng, Approaches to energy efficiency in air conditioning: a comparative study on purge configurations for indirect evaporative cooling, Energy 168 (2019) 505–515, https://doi.org/10.1016/j.energy.2018.11.077.

[23] Y. Min, Y. Chen, H. Yang, A statistical modeling approach on the performance prediction of indirect evaporative cooling energy recovery systems, Appl. Energy 255 (2019) 113832, https://doi.org/10.1016/j.apenergy.2019.113832.
[24] Y. Min, Y. Chen, H. Yang, C. Guo, Characteristics of primary air condensation in indirect evaporative cooler: theoretical analysis and visualized validation, Build. Environ. 174 (2020) 106783, https://doi.org/10.1016/j.buildenv.2020.106783.
[25] A. Tejero-González, M. Andrés-Chicote, E. Velasco-Gómez, F.J. Rey-Martínez, Influence of constructive parameters on the performance of two indirect evaporative cooler prototypes, Appl. Therm. Eng. 51 (2013) 1017–1025, https://doi.org/10.1016/j.applthermaleng.2012.10.054.
[26] A. Cichoń, A. Pacak, D. Pandelidis, S. Anisimov, Reducing energy consumption of air-conditioning systems in moderate climates by applying indirect evaporative cooling, in: E3S Web Conf, 2018.
[27] A. Khalid, M. Mahmood, M. Asif, T. Muneer, Solar assisted, pre-cooled hybrid desiccant cooling system for Pakistan, Renew. Energy 34 (2009) 151–157, https://doi.org/10.1016/j.renene.2008.02.031.
[28] Y. Chen, Y. Luo, H. Yang, Energy saving potential of hybrid liquid desiccant and evaporative cooling air-conditioning system in Hong Kong, Energy Procedia 105 (2017) 2125–2130, https://doi.org/10.1016/j.egypro.2017.03.601.
[29] W. Ahmad, M. Ali, N.A. Sheikh, J. Akhtar, Effect of efficient multi-stage indirect evaporative cooling on performance of solar assisted desiccant air conditioning in different climatic zones, Heat Mass Transf. 56 (2020) 2725–2741, https://doi.org/10.1007/s00231-020-02900-2.
[30] X. Cui, K.J. Chua, M.R. Islam, K.C. Ng, Performance evaluation of an indirect pre-cooling evaporative heat exchanger operating in hot and humid climate, Energy Convers. Manag. 102 (2015) 140–150, https://doi.org/10.1016/j.enconman.2015.02.025.
[31] S. Delfani, J. Esmaeelian, H. Pasdarshahri, M. Karami, Energy saving potential of an indirect evaporative cooler as a pre-cooling unit for mechanical cooling systems in Iran, Energy Build. 42 (2010) 2169–2176.
[32] X. Cui, L. Sun, S. Zhang, L. Jin, Study of a hybrid indirect evaporative pre- cooling system for various climates, Energies 12 (2019) 4419.
[33] X. She, Y. Yin, Y. Dong, X. Zhang, Investigation on air flow patterns of evaporative cooling and dehumidification process for a hybrid refrigeration system, Appl. Therm. Eng. 95 (2016) 79–94, https://doi.org/10.1016/j.applthermaleng.2015.11.044.
[34] C. Cianfrini, M. Corcione, E. Habib, A. Quintino, Energy performance of air-conditioning systems using an indirect evaporative cooling combined with a cooling/reheating treatment, Energy Build. 69 (2014) 490–497, https://doi.org/10.1016/j.enbuild.2013.11.030.
[35] Y. Al-Horr, B. Tashtoush, N. Chilengwe, M. Musthafa, Performance assessment of a hybrid vapor compression and evaporative cooling fresh-air-handling unit operating in hot climates, Processes 7 (2019) 1–21.
[36] Z. Duan, X. Zhao, J. Liu, Q. Zhang, Dynamic simulation of a hybrid dew point evaporative cooler and vapour compression refrigerated system for a building using EnergyPlus, J. Build. Eng. 21 (2019) 287–301, https://doi.org/10.1016/j.jobe.2018.10.028.
[37] M.H. Mahmood, M. Sultan, T. Miyazaki, S. Koyama, V.S. Maisotsenko, Overview of the Maisotsenko cycle – a way towards dew point evaporative cooling, Renew. Sust. Energ. Rev. 66 (2016) 537–555, https://doi.org/10.1016/j.rser.2016.08.022.
[38] P.M. Cuce, S. Riffat, A state of the art review of evaporative cooling systems for building applications, Renew. Sust. Energ. Rev. 54 (2016) 1240–1249, https://doi.org/10.1016/j.rser.2015.10.066.
[39] T. Sun, X. Huang, Y. Chen, H. Zhang, Experimental investigation of water spraying in an indirect evaporative cooler from nozzle type and spray strategy perspectives, Energy Build. 214 (2020) 109871.
[40] K. Rajski, J. Danielewicz, E. Brychcy, Performance evaluation of a gravity-assisted heat pipe-based indirect evaporative cooler, Energies 13 (2020) 1–20.
[41] S. De Antonellis, L. Cignatta, C. Facchini, P. Liberati, Effect of heat exchanger plates geometry on performance of an indirect evaporative cooling system, Appl. Therm. Eng. 173 (2020) 115200, https://doi.org/10.1016/j.applthermaleng.2020.115200.
[42] M.W. Shahzad, M. Burhan, D. Ybyraiymkul, S.J. Oh, K. Choon, An improved indirect evaporative cooler experimental investigation, Appl. Energy 256 (2019) 113934, https://doi.org/10.1016/j.apenergy.2019.113934.
[43] B. Zheng, C. Guo, T. Chen, Q. Shi, J. Lv, Y. You, Development of an experimental validated model of cross-flow indirect evaporative cooler with condensation, Appl. Energy 252 (2019) 113438, https://doi.org/10.1016/j.apenergy.2019.113438.
[44] D. Meng, J. Lv, Y. Chen, H. Li, X. Ma, Visualized experimental investigation on cross-flow indirect evaporative cooler with condensation, Appl. Therm. Eng. 145 (2018) 165–173, https://doi.org/10.1016/j.applthermaleng.2018.09.026.
[45] J. Lv, D. Meng, Y. Chen, Y. You, H. Li, An experimental study on condensate film of indirect evaporative cooler, Energy Proc. 158 (2019) 5753–5758, https://doi.org/10.1016/j.egypro.2019.01.556.
[46] Y. Chen, H. Yang, Y. Luo, Parameter sensitivity analysis of indirect evaporative cooler (IEC) with condensation from primary air, Energy Proc. 88 (2016) 498–504, https://doi.org/10.1016/j.egypro.2016.06.069.
[47] Y. Chen, H. Yang, Y. Luo, Indirect evaporative cooler considering condensation from primary air: model development and parameter analysis, Build. Environ. 95 (2015) 330–345, https://doi.org/10.1016/j.buildenv.2015.09.030.
[48] M. Guilizzoni, S. Milani, P. Liberati, S. De Antonellis, Effect of plates coating on performance of an indirect evaporative cooling system Effet de l'enrobage des plaques sur les performances d'un système de refroidissement évaporatif indirect, Int. J. Refrig. 104 (2019) 367–375, https://doi.org/10.1016/j.ijrefrig.2019.05.029.
[49] C. Guo, B. Zheng, Experimental study on evaluation index of indirect evaporative cooling heat transfer performance cooling heat transfer performance assessing the feasi, Energy Proc. 158 (2019) 5789–5794, https://doi.org/10.1016/j.egypro.2019.01.550.
[50] F. Comino, M.R. De Adana, Very low energy consumption HVAC systems for NZEB buildings. The potential of indirect evaporative coolers in South European climates Very low energy consumption HVAC systems for NZEB buildings. The potential of indirect evaporative coolers in South Eur, in: Int. Conf. Green Constr., Cordoba, Spain, 2019.
[51] S. De Antonellis, C.M. Joppolo, P. Liberati, Performance measurement of a cross-flow indirect evaporative cooler: effect of water nozzles and airflows arrangement, Energy Build. 184 (2019) 114–121, https://doi.org/10.1016/j.enbuild.2018.11.049.
[52] S. De Antonellis, C.M. Joppolo, P. Liberati, S. Milani, F. Romano, Modeling and experimental study of an indirect evaporative cooler, Energy Build. 142 (2017) 147–157, https://doi.org/10.1016/j.enbuild.2017.02.057.
[53] S. De Antonellis, C.M. Joppolo, P. Liberati, S. Milani, L. Molinaroli, Experimental analysis of a cross flow indirect evaporative cooling system, Energy Build. 121 (2016) 130–138, https://doi.org/10.1016/j.enbuild.2016.03.076.
[54] F. Wang, T. Sun, X. Huang, Y. Chen, H. Yang, Experimental research on a novel porous ceramic tube type indirect evaporative cooler, Appl. Therm. Eng. 125 (2017) 1191–1199, https://doi.org/10.1016/j.applthermaleng.2017.07.111.
[55] Z. Duan, X. Zhao, J. Li, Design, fabrication and performance evaluation of a compact regenerative evaporative cooler: towards low energy cooling for buildings, Energy 140 (2017) 506–519, https://doi.org/10.1016/j.energy.2017.08.110.
[56] Z. Duan, C. Zhan, X. Zhao, X. Dong, Experimental study of a counter-flow regenerative evaporative cooler, Build. Environ. 104 (2016) 47–58, https://doi.org/10.1016/j.buildenv.2016.04.029.
[57] A. Ahmad, S. Rehman, L.M. Al-Hadhrami, Performance evaluation of an indirect evaporative cooler under controlled environmental conditions, Energy Build. 62 (2013) 278–285, https://doi.org/10.1016/j.enbuild.2013.03.013.
[58] J. Lee, D.Y. Lee, Experimental study of a counter flow regenerative evaporative cooler with finned channels, Int. J. Heat Mass Transf. 65 (2013) 173–179, https://doi.org/10.1016/j.ijheatmasstransfer.2013.05.069.
[59] J. Lin, R.Z. Wang, M. Kumja, T.D. Bui, K.J. Chua, Modelling and experimental investigation of the cross-flow dew point evaporative cooler with and without dehumidification, Appl. Therm. Eng. 121 (2017) 1–13, https://doi.org/10.1016/j.applthermaleng.2017.04.047.
[60] A.E. Kabeel, M.M. Bassuoni, M. Abdelgaied, Experimental study of a novel integrated system of indirect evaporative cooler with internal baffles and evaporative condenser, Energy Convers. Manag. 138 (2017) 518–525, https://doi.org/10.1016/j.enconman.2017.02.025.
[61] K.J. Chua, J.X.X. Cui, K.C.N.M.R. Islam, Numerical heat and mass transfer analysis of a cross - flow indirect evaporative cooler with plates and flat tubes, Heat Mass Transf. 52 (2015) 1765–1777, https://doi.org/10.1007/s00231-015-1696-y.
[62] M.W. Shahzad, J. Lin, B. Bin Xu, L. Dala, Q. Chen, M. Burhan, M. Sultan, W. Worek, K.C. Ng, A spatiotemporal indirect evaporative cooler enabled by transiently interceding water mist, Energy 217 (2020) 119352, https://doi.org/10.1016/j.energy.2020.119352.
[63] S. Kakac, H. Liu, Heat Exchangers: Selection, Rating, and Thermal Design, 2nd ed., CRC, New York, 2002.
[64] I.S. Hussaini, S.M. Zubair, M.A. Antar, Area allocation in multi-zone feedwater heaters, Energy Convers. Manag. 48 (2007) 568–575, https://doi.org/10.1016/j.enconman.2006.06.003.
[65] J.H. Kim, T.W. Simon, Journal of heat transfer policy on reporting uncertainties in experimental measurements and results, J. Heat Transf. 115 (1993) 5–6, https://doi.org/10.1115/1.2910670.
[66] M.A. Jamil, Z.U. Din, T.S. Goraya, H. Yaqoob, S.M. Zubair, Thermal-hydraulic characteristics of gasketed plate heat exchangers as a preheater for thermal desalination systems, Energy Convers. Manag. 205 (2020) 112425, https://doi.org/10.1016/j.enconman.2019.112425.
[67] B.A. Qureshi, S.M. Zubair, A comprehensive design and rating study of evaporative coolers and condensers. Part II. Sensitivity analysis, Int. J. Refrig. 29 (2006) 659–668.
[68] M.A. Jamil, T.S. Goraya, M.W. Shahzad, S.M. Zubair, Exergoeconomic optimization of a shell-and-tube heat exchanger, Energy Convers. Manag. 226 (2020) 113462, https://doi.org/10.1016/j.enconman.2020.113462.
[69] B.N. Taylor, C.E. Kuyatt, Guidelines for Evaluating and Expressing the Uncertainty of NIST Measurement Results, U.S. Departmente of Commerce, Technology Administration, National Institute of Standards and Technology, Gaithersburg, MD, 1994.
[70] M. Masi, S. Fogliani, S. Carrà, Sensitivity analysis on indium phosphide liquid encapsulated Czochralski growth, Cryst. Res. Technol. 34 (1999) 1157–1167.

[71] C.A. James, R.P. Taylor, B.K. Hodge, The application of uncertainty analysis to cross-flow heat exchanger performance predictions, Heat Transf. Eng. 16 (1995) 50–62.
[72] C.A. James, R.P. Taylor, B.K. Hodge, Analysis and Design of Energy Systems, 3rd ed., Prentice Hall, Englewood Cliffs, NJ, 1998.
[73] B. Givoni, Man, Climate, and Architecture, Elsevier Publishing Company Limited, Amsterdam; London; New York, 1969.
[74] B. Givoni, Comfort, climate analysis and building design guidelines, Energy Build. 18 (1992) 11–23, https://doi.org/10.1016/0378-7788(92)90047-K.
[75] V. Olgyay, Design With Climate: Bioclimatic Approach to Architectural Regionalism, Princeton University Press, 2015. https://press.princeton.edu/books/paperback/9780691169736/design-with-climate (accessed January 23, 2021).
[76] K. Vadoudi, S. Marinhas, Development of Psychrometric diagram for the energy efficiency of Air Handling Units, Int. J. Vent. 3 (2018) 491–500.